Technische Universität Dortmund

Physics Department

International Master Advanced Methods in Particle Physics

Characterization Of Scintillating Fibres

Laboratory report

Date: May 28, 2024

Simone Garnero - simone.garnero@tu-dortmund.de

Bastian Schuchardt - bastian.schuchardt@tu-dortmund.de

Dortmund, Germany May, 2024

Contents

Measurement of scintillating fibres for the LHCb experiment

Advanced Laboratory Course: Particle Physics

Simone Garnero, Bastian Schuchardt

May 28, 2024

Abstract

The objective of this laboratory experiment is to determine the properties of scintillating fibers and explain their usage in tracking detectors for high-energy physics in detectors like LHCb. Already existing simulations will be compared to the measurements.

1 Introduction

Tracking detectors play a great role in analyzing collision experiments by determining the tracks, momentum, and charge of particles that pass through them. With this information and the help of calorimeters and muon chambers events at e.g. the LHCb can be properly reconstructed. Moreover, tracking detectors can be realized by scintillating fibers that get excited when a charged particle passes through them. After the excitation, the fiber emits photons that can be detected with silicon photomultipliers

1.1 LHCb

The LHCb experiment is one of the four largest experiments at the Large Hadron Collider (LHC) at CERN and is used to further investigate the decay of hadrons with either a bottom- or charm-quark, various rare decays, and precision measurements of the standard model. In addition, the experiment probes CP-violation and searches for reasons for the matter-antimatter asymmetry in the universe. The structure of the LHCb detector is given in Figure 1. The detector consists of various subdetectors like the vertex locator VELO, the Cherenkov detectors RICH1 and RICH2 that allow computing the momentum of the particle, the SciFi Tracker, the two calorimeters ECAL and HCAL, and the four muon chamber M2-M5.

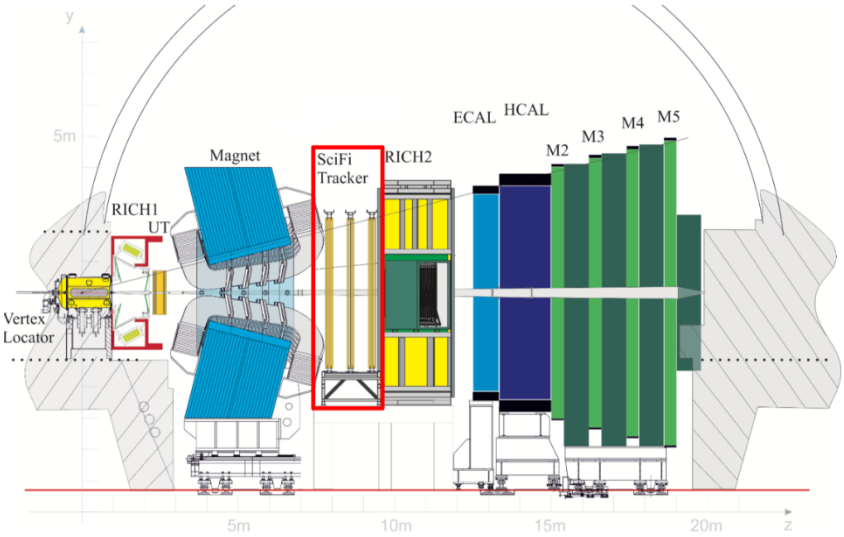

Figure 1: Schematic structure of the LHCb detector. From left to right the vertex detector VELO, the cherenkov detectors RICH1 and RICH2, the SciFi Tracker highlighted with a red box, the electromagnetic and hadronic calorimeter, and the muon chambers can be seen. [1]

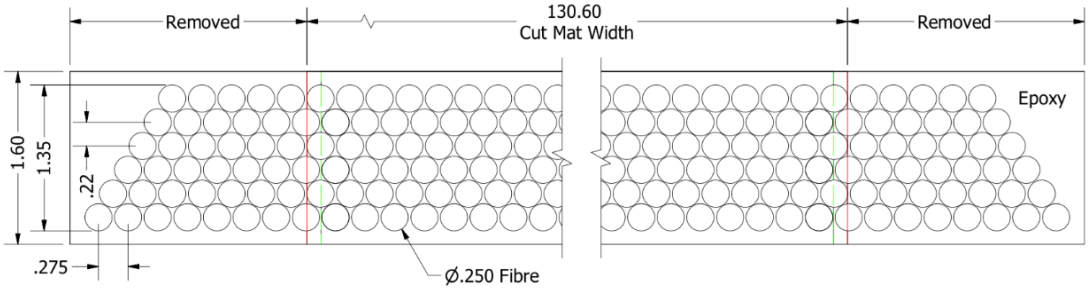

Figure 2: Schematic cross section of a fibre mat. The mat consists of six layers in a hexagonal structure. [2]

1.2 Scintillating Fibre Tracker

In the Scintillating Fibre Tracker (SciFi Tracker) scintillating fibres are produced in fibre mats that can be seen in Figure 2. In the SciFi Tracker the mats are ordered in a $x-u-v-x$ pattern where the u and v layers are tilted by 5° sideways to get a better resolution. Each layers has 40 mats and two on top of each other. Overall, the SciFi Tracker has three stations with these four layers each. To maximize the photon yield mirrors have been put between the mats.

1.3 Scintillating fibres

The used fibres have a total thickness of 250 µm and have a polystyrene core with a thickness of 220 µm and two sheaths with a thickness of 7.5 µm each. With these fibres a resolution of under 100 µm can be achieved. This can be explained by the structure of the fibre that is

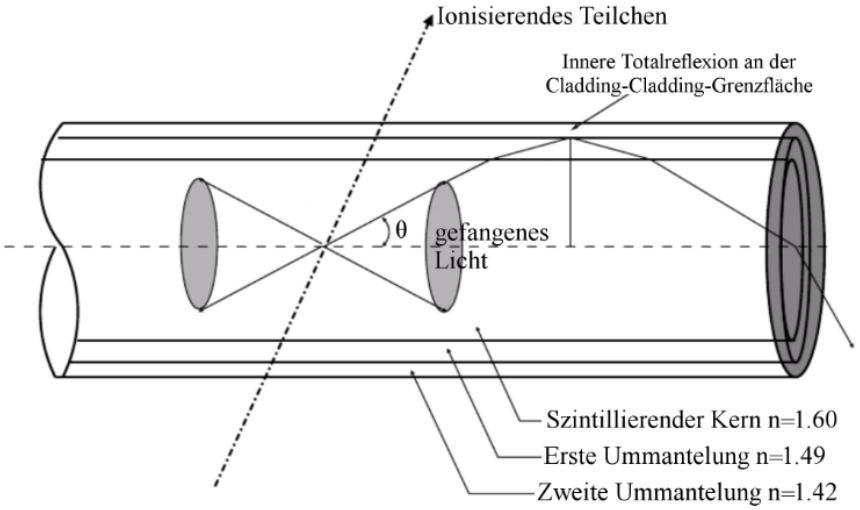

Figure 3: Schematic of a fibre, after an ionizing particle hits the core and the core, emits a photon that travels through the fibre. [1]

uniformly distributed over the given thickness. The standard deviation for a uniform distribution according to the fibre yields $\sigma = \sqrt{\frac{(250\,\mu\text{m})^2}{12}} = 72.17\,\mu\text{m}$. From this it can be followed that most interactions of the particle with the fibre happen within one standard deviation and the desired resolution can be achieved.

The schematic structure of an excited fibre can be seen in Figure 3. When a charged particle ionizes the core, the core emits a photon deexcites. The photon now travels through the fibre by total internal reflection at the Cladding-Cladding surface between the two sheaths. To ensure that the photons have a long enough attenuation length a tetraphenyl-butadiene was used as a wavelength shifter in the fibre.
From simple optics, the path length of a photon that travels through the fibre can be derived to be

$$L = \frac{x}{\cos\theta}\,, \tag{1}$$

where x is the length to the end of the fibre and θ the angle of the emitted photon measured from the center axis of the core. Furthermore, the number of times the photon gets reflected N can be computed from

$$N = \frac{x\tan\theta}{2\sqrt{r_{\text{core}}^2 - r_{\text{min}}^2}}\,, \tag{2}$$

where r_{core} is the radius of the core and r_{min} is the smallest distance path to the center axis of the core. For the refractive indexes $n_{\text{core}} = 1.60$ and $n_1 = 1.49$ given in Figure 3 the maximal angle for total internal reflection to occur is 68.63°.

1.4 Absorption

Not all photons reach the end of the fibre because of reflections at the end of the fibre or at the sheaths. Other possible effects of this behaviour are Rayleigh scattering or absorption.

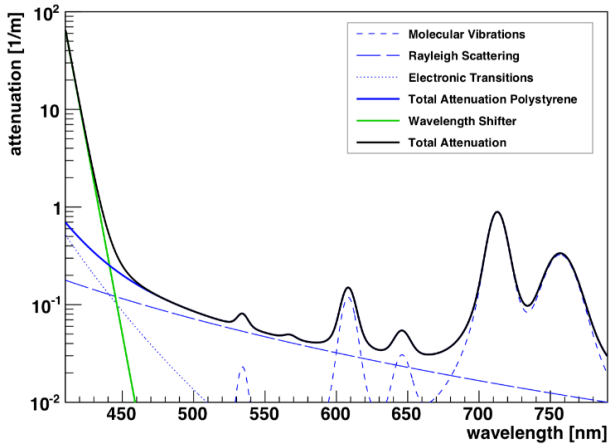

Figure 4: Influence of various effects on the attenuation coefficient in the core for different wavelengths. Reflection losses are neglected in this plot. [1]

The influence of these effects on the attenuation coefficient at different wavelengths is given in Figure 4.
The reflection losses and the photon losses in the core can be summarized in one effective attenuation coefficient

$$a_{eff} = \frac{a_0}{\cos\theta} + \frac{\epsilon \tan\theta}{2\sqrt{r_{\text{core}}^2 - r_{\text{min}}^2}}\,, \tag{3}$$

where a_{eff} is the effective attenuation coefficient and ϵ the reflection coefficient. The attenuation length is the inverse of the attenuation coefficient a.

2 Experiment

Measurements are taken on a single optical fibre that can be excited by an LED. The LED can be shifted along the x axis and the spectrometer that is attached at to the end of the fibre can be shifted in the horizontal and vertical plane. All measurements are taken in the dark and are controlled by a computer.

Before every measurement, a reference run was done to test that the experiment works properly.

2.1 Simulation

To compare the measurements, Monte Carlo generated data is given. For the simulation, a single fibre with photons that move through it was implemented in GEANT4. 50 fibres in total have been excited at 24 different spots with a distance from 2400 mm to 100 mm to the fibre end, for a total of 1200 simulated excitations, each one of these with several photons detected. The simulation has the following features: start-/exit-position and momentum along the x, y, and z axis, the number of reflections at the core-cladding or cladding-cladding interface, the x-coordinate where the primary particle for the excitation was created, the

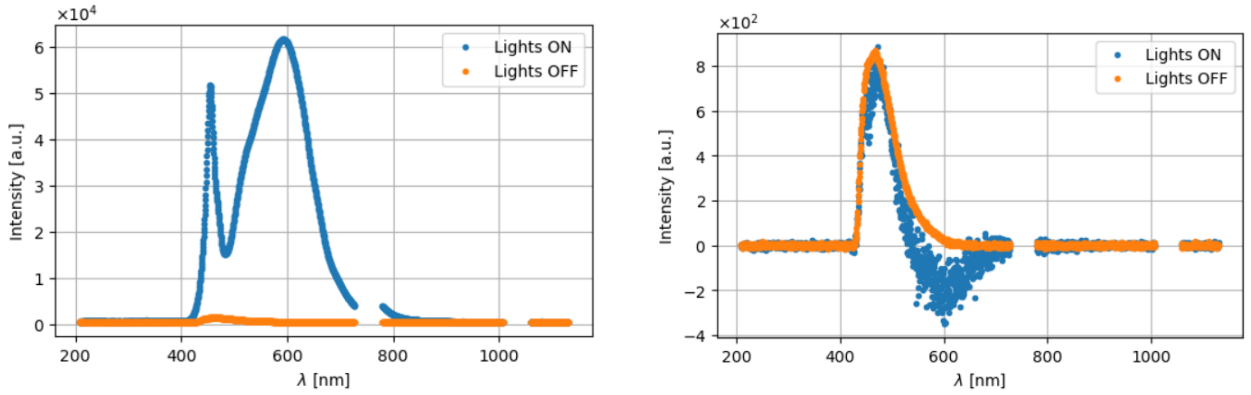

(a) Measured intensity

(b) Adjusted intensity

Figure 5: LED signal intensity measured under ambient light conditions and in the absence of room light. In (a) the intensity is plotted as it has been measured, while in (b) the signal is adjusted by subtracting the dark counts (data taken in the absence of signal) from the normal signal.

distance traveled in the core or the cladding, and the number of Rayleigh scatterings that the photon experienced on its way through the fibre.

2.2 Dataset

For the experimental data collected in the laboratory, we have a large number of files for each measurement. For example, a single file contains the signal at a horizontal angle of 0°, a vertical angle of 18°, a distance of 1200 mm, and so forth. Each file includes only two features: the wavelength λ and the intensity count. This means that each file contains a signal of the type depicted in Figure 5.
As mentioned earlier, for the simulation data, we had a total of 1200 files, each representing a single excitation at a different point on a fiber and containing several photons and many features. Unfortunately, during the downloading procedure of these simulation files, some of them were corrupted. The number of corrupted files is 45 out of a total of 1200, representing only 3.75% of the sample, and they are randomly distributed. We decided then to simply ignore the corrupted files and work with the remaining 96.25% of the total.

3 Measurements and Analysis

3.1 Experimental analysis

3.1.1 Spectrometer measurement

The first measurement conducted involved a spectrometer. Its purpose was to check the instrument's behavior, initially with room light on and then off. This was carried out using a graphical user interface (GUI) on the lab computer. The intensity counts were plotted against the light wavelength for both scenarios. In Figure 5, the outcomes of this assessment

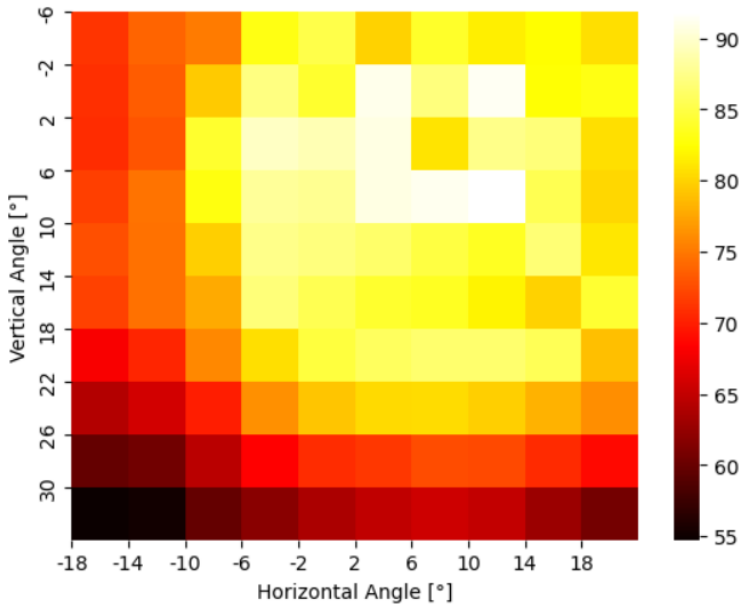

Figure 6: Radial intensity distribution with respect to the horizontal and the vertical angles, the colour represents the measured intensity level.

are depicted. Specifically, in Figure 5a, the LED signal is presented under both illuminated and darkened conditions. Furthermore, in Figure 5b, the preceding assessment is refined by subtracting the dark count measurements. With this method, we can get rid of the big part of the background signal which would compromise our scientific results.

3.1.2 Radial symmetry measurement

After that, a radial symmetry measurement has been taken to verify the symmetry of the light intensity. In order to achieve this, the light intensity has been recorded for several different angles but with a fixed excitation position. That means that the spectrometer moved horizontally and vertically, while the LED was fixed at the same spot at 0 mm.
The horizontal angle covers a range of $[-18°; 30°]$, while the vertical one covers $[-6°; 35°]$. Hence, it has been decided to span from $-2°$ to $18°$ in the horizontal plane, with a step of $4°$, and from $-6°$ to $30°$ in the vertical plane, always with the same step of $4°$. In this way, a total of 100 measurements have been taken. The intensity has then been displayed in a two-dimensional histogram as a function of the two angles. By utilizing the dark count measurements, as done for the first task, we can eliminate part of the background to obtain the true distribution, as depicted in Figure 6. Since each measurement yields a signal resembling the one depicted in Figure 5, we have opted to utilize the maximum peak of the signal as the intensity value for our analysis. This choice is arbitrary; alternatively, the mean value could have been a suitable option.

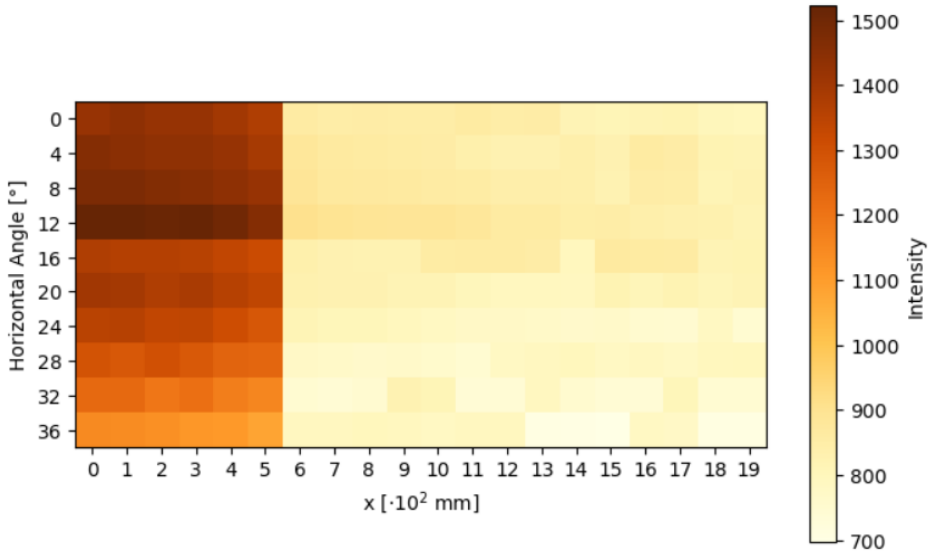

Figure 7: Light intensity as a function of the distance x from the end of the fiber and the horizontal angle. A point of discontinuity is visible at a height of approximately 550 mm; this is due to a fiber fracture.

3.1.3 Intensity measurement

Subsequently, we carried out intensity measurements by changing the horizontal angle and the excitation position. For the angle, 10 steps of 4° within the range $[0°; 40°]$ have been selected. For each of these angles, the fiber has been excited at 20 different points, spaced by 100 mm intervals from 0 to 2 m, for a total of 200 measurements. The results are shown in a 2D histogram in Figure 7, which indeed represents the light intensity as a function of both the x distance and the horizontal angle.

3.1.4 Small angles intensity measurement

Finally, an intensity measurement for small angles was conducted, while keeping the excitation location and the vertical angle constant and varying the horizontal angle in small steps of 1° between 0° and 40°. In Figure 8, one can observe a histogram showing the intensity measured for each angle. The red bin represents the angle that recorded the highest number of photons.

3.2 Simulation analysis

Regarding the analysis of the Monte Carlo simulation, initially, the 1200 files were merged to create a unified dataset. Subsequently, the dataset underwent preprocessing to remove photons responsible for Rayleigh scattering and those with a distance between the exit point and the fiber center exceeding the fiber radius. Following this, the dataset was partitioned into two subsets: one comprising solely core photons and the other exclusively containing cladding photons. Utilizing the momentum of each photon, which is standardized as $p_x^2 + p_y^2 + p_z^2 = p^2$, and is one of the features in the dataset, the angle θ of the photon to the x-axis

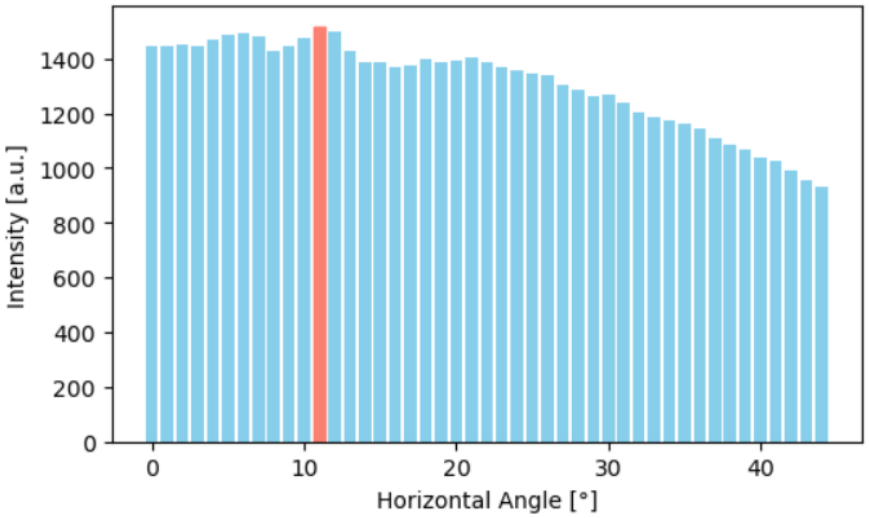

Figure 8: Histogram illustrating the measured intensity for small horizontal angles. The red bin corresponds to the highest count of photons recorded.

of the fiber has been calculated and incorporated into the dataset. After that, we computed the maximum angle at which total internal reflection can still occur for core photons and cladding photons, simply reiterating Snell's law:

$$n_1 \sin(\theta_1) = n_2 \sin(\theta_2) \tag{4}$$

We obtain

$$\theta_{\text{max}}^{\text{core}} = 21.37°$$
$$\theta_{\text{max}}^{\text{clad}} = 27.44°.$$

In Figure 9, the two histograms with the θ distributions respectively for core and cladding photons are shown. Additionally, the theoretical maximum angles have been highlighted. As a next step, the minimum distance of the photons to the fiber centre has been determined and added to the dataset. This has been done by an analytical argument: we considered the feature r_{min}, which we want to compute, as the distance between two skew lines in a 3-dimensional space. The first line is given by the x-axis of the fiber (the centre of the fiber) and the other by the trajectory of the photon. In Figure 10 the distributions of r_{min} for the angle θ for both core and cladding photons are depicted.
Afterward, the intensity has been determined for different angles as a function of the excitation position. This has been achieved using a two-dimensional histogram (Figure 11) with the feature of the dataset *gpsPosX* and the angle θ.

3.2.1 Attenuation coefficient

Eventually, an exponential fit was employed to ascertain the attenuation coefficient as a function of the distance. In Figure 12, one can observe an attempt to compare the attenuation coefficient for the different angles of the simulation to the one obtained by the experimental

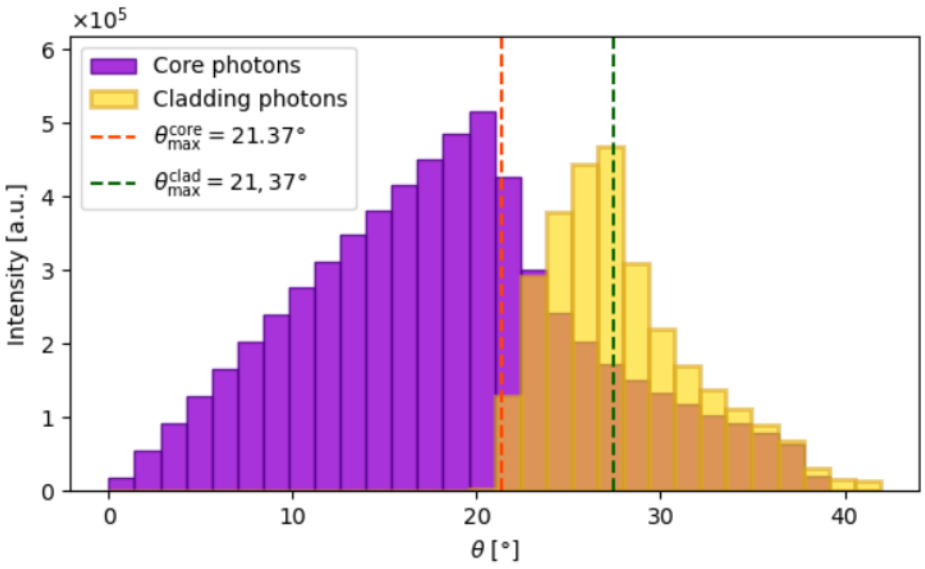

Figure 9: Angular distribution of photons from the simulation, categorized by core and cladding. The two dashed lines denote the theoretical maximum angles.

data. The goal of these two plots is indeed to fit them with the exponential function

$$I(x) = I_0 \exp\left(-\frac{L}{\Lambda}\right), \tag{5}$$

find the attenuation coefficient a, given by the inverse of the attenuation length Λ, and compare experimental data and simulation.
Unfortunately, the fracture in the fiber ruins the exponential behaviour of the intensity for the experimental data. An attempt to do two different fits for the two separated exponential parts of the function has been made, but the results were not acceptable. However, for the simulation data, this fit has been performed and the resultant attenuation coefficient, as a mean value between the different angles, is:

$$a_{avg,sim} = 2,04 \cdot 10^{-4} \frac{1}{\text{mm}} \tag{6}$$

4 Discussion

From the spectrometer measurement in Figure 5, it's evident that acquiring data in the absence of ambient light is crucial, and correcting by subtracting the dark counts is essential for obtaining a clean signal. During the "lights On" measurement, the background noise was significant to the extent that subtracting the dark counts from the signal resulted in values below zero, which is clearly unacceptable. The radially symmetric distribution of photons leaving the fiber is confirmed by the plot in Figure 6. Despite not having the complete spectrum, the behavior is evidently symmetric. An intriguing and significant observation is

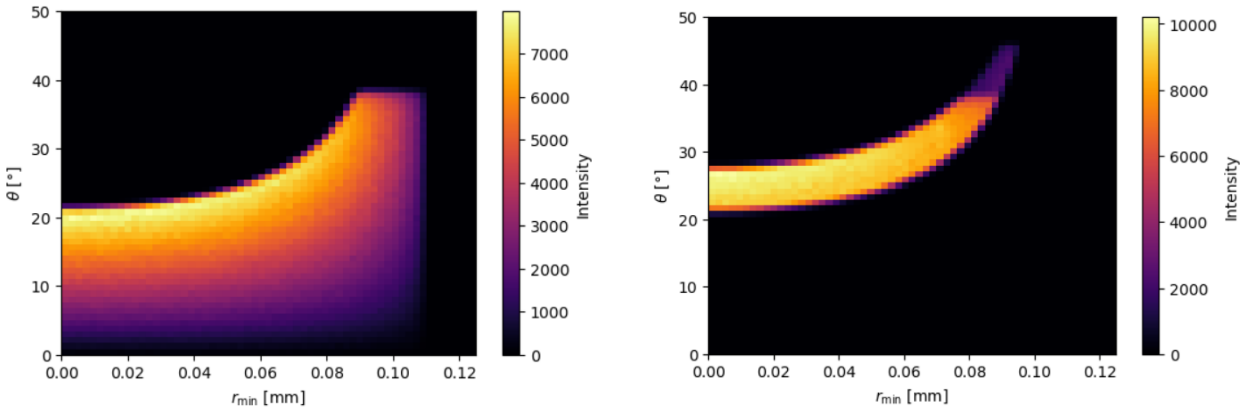

(a) Core photons

(b) Cladding photons

Figure 10: 2-dimensional histograms showing the behaviour of r_{min} with respect to the angle θ.

that the maximum intensity does not occur at 0°. The same concept is also demonstrated in Figure 7, where the peak is clearly observed around $\theta = 12°$. In this 2-dimensional histogram, another noteworthy observation is the discontinuity point at approximately 550 mm. This abrupt change in behavior is not natural and is attributed to a fracture in the fiber. The expected trend should resemble that of the simulation data, as depicted in a comparable plot in Figure 11. From these two graphs, we derived the ones depicted in Figure 12, essentially illustrating the same intensity behaviour as a function of distance and angle. From the simulation data, we were also able to calculate the attenuation coefficient as shown in Equation (6). However, the precision of the result may be compromised due to the continuous nature of angles in the simulation, which we discretized to make them comparable with the experimental data. In Figure 8 we observe that the angle which receives more photons is $\theta = 11°$, but we also see that the angles smaller than that have only a minimum difference level compared to the first. This could mean that with a longer measurement and a greater sample, the result could be different.
Regarding the simulation data, they can be categorized into core and cladding photons, each exhibiting distinct angle distributions as visualized in Figure 9. These distinctions are further elucidated in Figure 10, where the photons are depicted as functions of angle and the value of $r_{\min}$, which represents the minimum distance from the x-axis of the fiber and remains a constant parameter throughout the photon's trajectory. The observed distributions demonstrate a logical pattern, with larger values of $r_{\min}$ corresponding to larger angles, and vice versa.

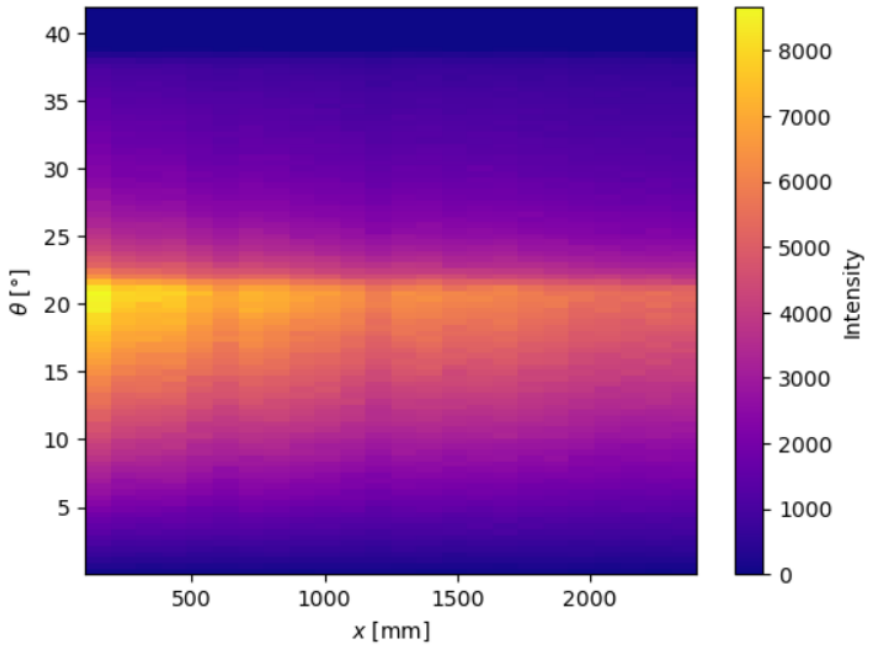

Figure 11: Attenuation of the signal in the fiber as a function of the angle for the simulation data. This plot is the equivalent of the one in Figure 7 but for the simulation data.

5 Conclusion

In conclusion, this analysis has provided a detailed overview of fundamental characteristics regarding the behavior of light intensity in optical fibers, drawing from both experimental data and simulations. From the results obtained in experimental measurements, the importance of acquiring data under controlled conditions and eliminating background noise through dark count subtraction has been evident. Furthermore, a radially symmetric distribution of photons emitted from the fiber was observed, with significant intensity peaks at angles not necessarily coinciding with zero. This observation was further corroborated through simulations, allowing for a precise categorization between core and cladding photons based on their angular distributions. Analysis of angular distributions for the minimum distance from the fiber axis revealed a direct relationship between this parameter and emission angles. The attenuation coefficient has been successfully computed for the simulation. However, it should be noted that the accuracy of simulation results might be limited by the discretization of angles necessary to make them comparable with experimental data. In summary, this work has deepened our understanding of light behavior in optical fibers, underlining the importance of proper acquisition and analysis of experimental data, as well as the utility of simulations in exploring real-life phenomena and emphasizing trends observed experimentally.

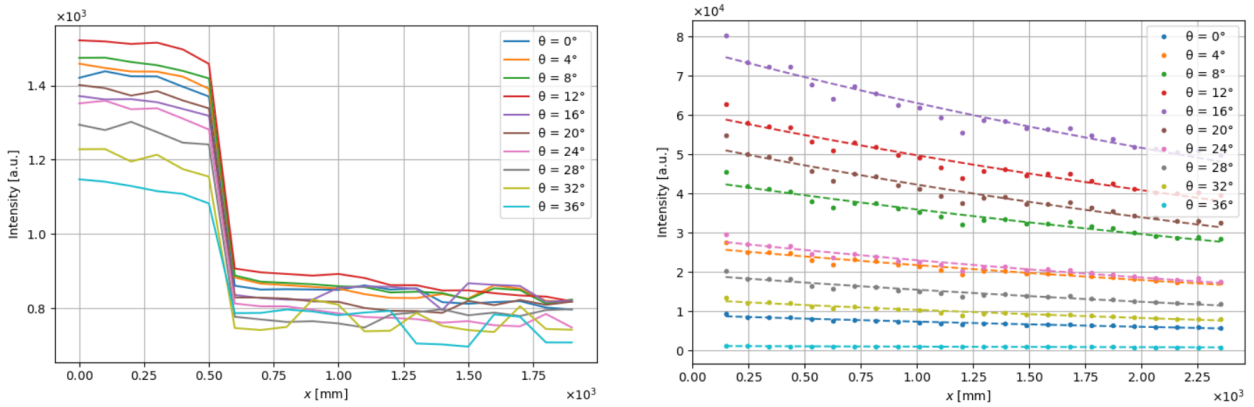

(a) Experimental data

(b) Simulation data

Figure 12: Plots showing the intensity trend as a function of the distance x from the end of the fiber for the experimental data (a) and the simulation (b) for 10 different angles. In (a), one can better appreciate the crack on the fiber that determines a sudden fall of intensity. In (b), an exponential fit for each angle has been performed to obtain the attenuation coefficient.

References

[1] LHCb Collaboration. LHCb Tracker Upgrade Technical Design Report. Technical report, 2014.

[2] Christian Joram, Ulrich Uwer, Blake Dean Leverington, Thomas Kirn, Sebastian Bachmann, Robert Jan Ekelhof, and Janine Müller. LHCb Scintillating Fibre Tracker Engineering Design Review Report: Fibres, Mats and Modules. Technical report, CERN, Geneva, 2015.